Journal of Materials Chemistry A

COMMUNICATION

View Article Online
View Journal

Cite this: DOI: 10.1039/d5ta03829d

Redox-mediated bipolar hydrogen production and furoic acid electrosynthesis

Hyunjoon Ji,[ab] Siqi Niu,[a] Changkun Zhang *[a] and Xianfeng Li *[a]

Received 13th May 2025
Accepted 24th July 2025

DOI: 10.1039/d5ta03829d

rsc.li/materials-a

Hydrogen production coupled with electrosynthesis is one of the promising strategies for upgrading traditional water electrolysis with reduced energy consumption. However, this coupling concept always needs a separate time-consuming discharge process to restore the mediator, thus lowering the hydrogen productivity. Herein, we propose a novel three-chamber cell design to achieve continuous anodic and cathodic hydrogen production coupled with furfural electrooxidation. Zinc or organic redox-active molecule mediators were applied to effectively store and release energy and hydrogen independently on demand. Simultaneous hydrogen production from two different chambers enabled a furfural-hydrogen conversion efficiency of 184% with high energy-storage flexibility. The three-chamber cell enabled 2-furoic acid yield of above 95%, while simultaneous cycling yielded 2-furoic acid above 88% for 24 h. Our cell concept enhanced the time and energy efficiency of furfural-hydrogen co-production.

Introduction

Hydrogen is the most abundant and lightest energy source on the Earth, with no associated concerns about resource depletion since it can be produced by water electrolysis without leaving any harmful byproducts.[1] Green hydrogen production powered by renewable energy sources like solar and wind power has been getting growing attention as a solution to decarbonize traditional industries.[2] One of the technical challenges to industrial-scale water electrolysis is the cost burden originating from the high water splitting voltage (>1.23 V) with sluggish oxygen evolution.[3] Research has been done on electrolyzer designs and non-noble metal-based catalysts to lower the high voltage required, thus reducing energy consumption and the cost.[4] One promising concept is combining hydrogen production with value-added electrosynthesis to generate hydrogen at a lower cell voltage and thereby improve the overall economic feasibility.[5] Various electrooxidation processes, ranging from using small molecules (*e.g.*, glucose,[6] furfural,[7] and alcohols[8]) to more sophisticated organic syntheses (oxidative coupling, dehydrogenation, and oxygenation), have been proposed.[5,9] Especially in terms of hydrogen production, biomass molecules containing aldehyde groups, such as formaldehyde,[10] furfural,[11] and hydroxymethylfurfural (HMF),[12] are considered suitable feedstocks due to their structural advantage of hydrogen self-generation. Combining the hydrogen evolution reaction (HER) with biomass reaction enables simultaneous hydrogen production from two different chambers.[13]

When water electrolysis is coupled with redox couples, the cell can store the energy in redox couples and release it later for power generation and hydrogen production on demand.[14] Such a rechargeable battery concept allows operational flexibility by decoupling two half-cell reactions. For example, hydrazine or ammonia oxidation was coupled with zinc redox reactions to generate hydrazine, ammonia, and hydrogen at the same anode with the help of bifunctional catalysts.[15] However, the cell needs a time-consuming periodic discharge to restore the mediator, and the low economic value of the nitrogen gas produced makes the cell less attractive. Coupling furfural redox cycling with a nickel-based redox couple in a closed-battery concept produced both furoic acid and furfural alcohol; however, the nickel cathode could only be used for redox reactions without achieving any valuable products such as hydrogen.[16] Therefore, developing a more efficient cell concept that is equipped with both energy storage and hydrogen production is still necessary.

The present work proposed a combination of furfural oxidation and hydrogen production in an energy-storage concept (Fig. 1a). A three-chamber cell was assembled using redox mediation (zinc or other soluble organic redox-active molecules). A furfural-hydrogen conversion efficiency of 184% and 2-furoic acid (2-FA) yield of 95% were achieved during separate single-flow cycling, while simultaneous operation produced a 2-FA yield of over 88% for 24 h. Furthermore, using

[a]Division of Energy Storage, Dalian National Laboratory for Clean Energy, Dalian Institute of Chemical Physics, Chinese Academy of Sciences, Dalian, 116023, China. E-mail: zhangchk17@dicp.ac.cn; lixianfeng@dicp.ac.cn
[b]University of Chinese Academy of Sciences, Beijing 100049, China

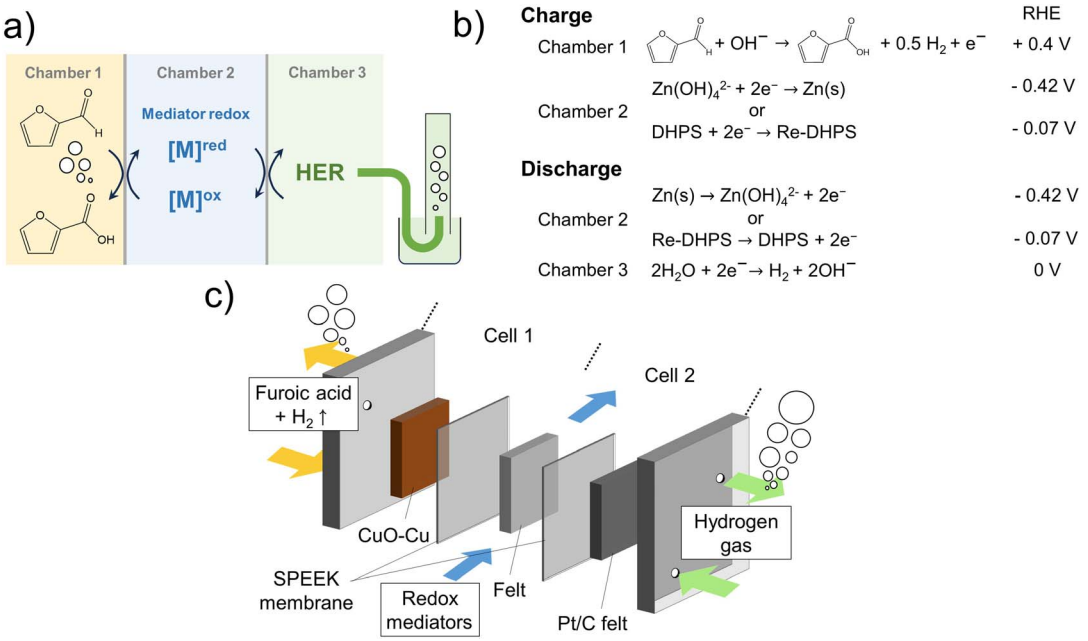

Fig. 1 Working concept of the three-compartment electroylsis cell. (a) Reactions in different chambers and (b) redox potential couplings in the three-chamber cell. Furfural oxidation (chamber 1) was coupled with zinc reduction (chamber 2) to form cell 1, while zinc oxidation (chamber 2) was combined with the HER (chamber 3) to form cell 2. (c) Schematic of the three-compartment cell assembly. The zinc mediator circulation was enabled between the furfural oxidation and HER chambers. A Cu catalyst electrode, graphite felt, and Pt/C catalyst-coated felt were placed in chambers 1, 2, and 3, respectively. Sulfonated poly(ether ether ketone) (SPEEK) membranes were used to separate each chamber and maintain the high purity of the products. Two channels were connected to cell 1 and cell 2, respectively, wherein counter electrodes of both the channels were connected to the zinc mediator compartment. A DHPS-based electrolyte circulation was enabled between the electrochemical reduction in chamber 2 and spontaneous chemical HER in chamber 3. The reduced state of DHPS (Re-DHPS) was re-oxidized back to DHPS when producing hydrogen.

7,8-dihydroxy-2-phenazinesulfonic acid (DHPS) mediator enabled electrolysis at 32% less energy consumption while maintaining the 2-FA yield above 92%. Our novel concept introduced a new possibility for time-efficient furfural-hydrogen co-production coupled with electrochemical energy-storage.

Results

The working concept of our three-chamber cell is displayed in Fig. 1a and b. Furfural can be oxidized into value-added furoic acid, simultaneously producing a half mole of hydrogen in the presence of a Cu catalyst in chamber 1.[11a] A mediator chamber 2 was sandwiched between the furfural oxidation and HER compartments (Fig. 1c). Zinc or the organic redox-active molecules (7,8-dihydroxy-2-phenazinesulfonic acid (DHPS), benzo[*a*] hydroxyphenazine-7,8-carboxylic acid (BHPC)), having low redox potentials at −1.25 V, −0.9 V, and −0.78 V *vs.* SHE in alkaline solutions, respectively, were used as mediator candidates (Fig. S1). $Zn(OH)_4^{2-}$ was reduced into solid Zn at the felt electrode during the furfural oxidation in cell 1 (pairing chamber 1 and chamber 2), and the deposited Zn was then oxidized back to $Zn(OH)_4^{2-}$ while simultaneously reducing hydrogen in cell 2 (pairing chamber 2 and chamber 3), enabling bipolar hydrogen production. Likewise, DHPS and BHPC can also be reduced in cell 1 and then re-oxidized in cell 2 to release hydrogen, where the water-soluble phase of both reduced and oxidized states of molecules enables high-energy-density energy storage.

Furfural electrooxidation

Furfural oxidation at the Cu electrocatalysts was initially achieved by growing $Cu(OH)_2$ nanotube precursors on the Cu foam, which were then thermally treated at 500 °C in air or argon to attain CuO and Cu_2O, respectively. The $Cu(OH)_2$–Cu, CuO–Cu, and Cu_2O–Cu electrocatalysts were obtained by electrochemically reducing $Cu(OH)_2$, CuO, and Cu_2O, respectively. Scanning electron microscopy (SEM) revealed that the CuO–Cu catalyst showed crystal defects along the nanotubes, while $Cu(OH)_2$–Cu revealed plain nanotubes, and Cu_2O–Cu showed nanotubes aggregated with each other (Fig. 2a and S2). X-ray diffraction (XRD) demonstrated that metallic Cu was the main phase for the three catalysts, and a small amount of Cu_2O was found in CuO–Cu (Fig. 2b), which was also observed in the transmission electron microscopy (TEM) images (Fig. 2c). Auger electron spectroscopy (AES) Cu LMM revealed a 1.9 eV difference between the two main peaks, implying that metallic Cu and Cu_2O coexist (Fig. S3). X-ray photoelectron spectroscopy (XPS) indicated the existence of metallic Cu, Cu_2O (including Cu(OH), indicating the existence of Cu^+),[17] and even traces of CuO in all the three samples (Fig. 2d). For the XPS O 1s spectra, an additional high peak was observed at around 532.9 eV for CuO–Cu, corresponding to adsorbed oxygen species from moisture or

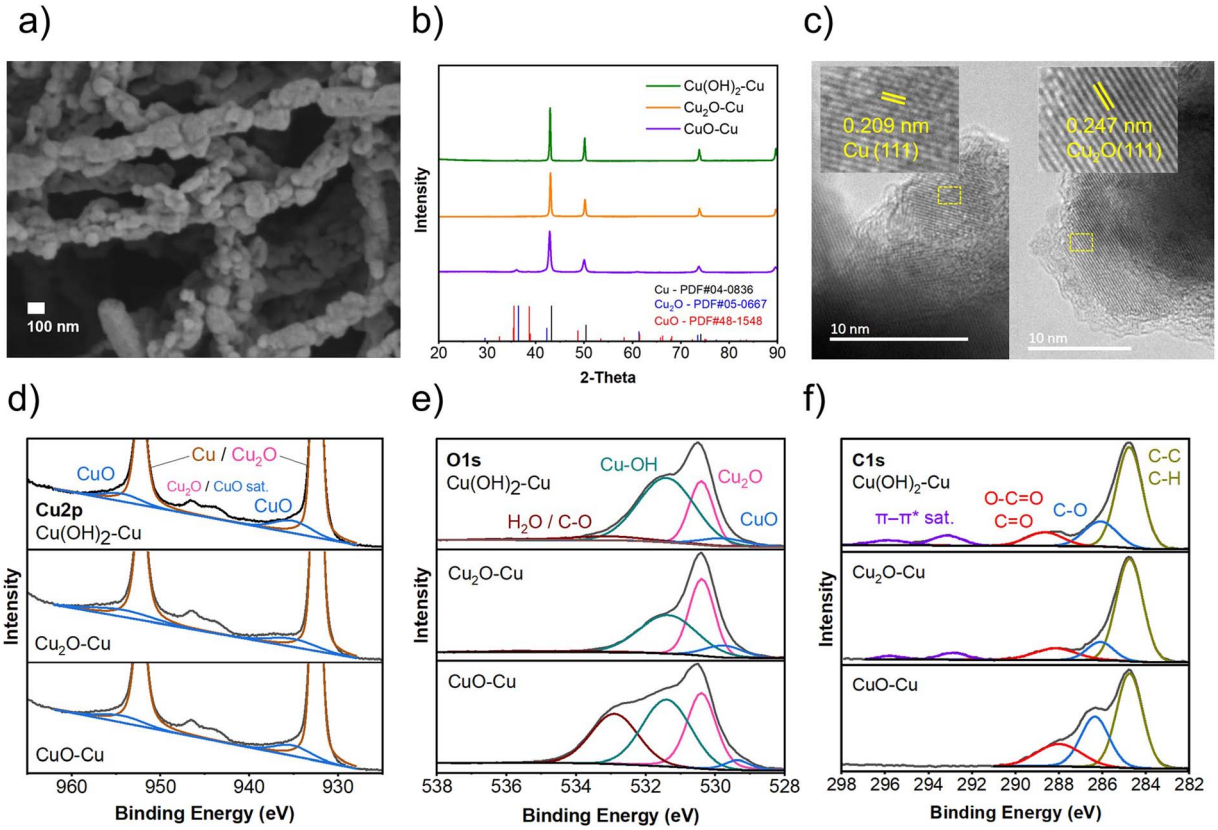

Fig. 2 Characterization of the Cu electrocatalysts. (a) SEM image of CuO–Cu, (b) XRD patterns of $Cu(OH)_2$–Cu, Cu_2O–Cu, and CuO–Cu electrocatalysts. (c) TEM images of CuO–Cu. (d) Cu 2p, (e) O 1s, and (f) C 1s XPS peak-fitting results of the three electrocatalysts. CuO–Cu reveals an exceptionally high O 1s peak at 532.9 eV.

organic adsorption (H_2O, C–O in Fig. 2e).[18] XPS C 1s spectra of CuO–Cu also revealed a higher portion of oxygen-bound adsorption (C–O, C═O, and COO–), while Cu_2O–Cu and $Cu(OH)_2$–Cu adsorbed π-conjugated aromatics at higher binding energies (π → π* shake-up), indicating the different adsorption behavior of the CuO–Cu electrocatalyst (Fig. 2f). Double-layer capacitance measurements in 1 M KOH also revealed that CuO–Cu showed a much higher current and capacitance than Cu_2O–Cu and $Cu(OH)_2$–Cu, implying its exceptional adsorption ability (Fig. S4). Vigorous oxygen removal during electrocatalyst preparation (electrochemical reduction) likely caused the reconstruction of the catalyst surface to increase the defects containing a higher population of Cu sites with low coordination numbers than $Cu(OH)_2$–Cu and Cu_2O–Cu, resulting in a strong adsorption energy.[19]

The furfural oxidation performance of different catalysts was evaluated by linear sweep voltammetry (LSV), and it has shown that a much higher current could be achieved using CuO–Cu than $Cu(OH)_2$–Cu and Cu_2O–Cu (Fig. 3a). The high current could be attributed to the richer population of defects and undercoordinated Cu sites, as mentioned above.[19a,20] Furthermore, the LSV current at different KOH concentrations increased along with the given potential, reaching a maximum current at 2 M KOH[11a] (Fig. S5). Cu itself also began to oxidize when the potential was above 0.45 V *vs.* RHE, thus the furfural chamber potential was fixed at 0.4 V *vs.* RHE for further experiments. When directly pairing furfural oxidation with the hydrogen evolution reaction (HER) at the anode in a flow cell, the furfural electrolyte was supplied in a continuous single-pass flow at an extremely slow flow rate of 1 mL min^{-1} to maximize the 2-FA yield (Fig. S6). Higher 2-FA yields were obtained with increasing the voltage (Fig. S7). Liquid chromatography-mass spectrometry (LC-MS) analysis revealed that using CuO–Cu at a cell voltage of 0.4 V, 2-FA was obtained as the main product, yielding 85% with a trace amount of furfuryl alcohol and 2-methylfuran (2-MF) as by-products due to the Cannizzaro disproportionation reaction (Fig. S8).

The stability of the catalysts was then evaluated in a furfural-HER flow cell, which was maintained at a constant cell voltage of 0.4 V for 10 hours. It was found that CuO–Cu maintained a current of above 20 mA cm^{-2} for 10 hours compared with the rapid current decrease observed for the $Cu(OH)_2$–Cu- and Cu_2O–Cu-based cells[11a,13] (Fig. 3b). The current fluctuations could be attributed to the more active hydrogen gas production on the catalyst surface. The surfaces of both $Cu(OH)_2$–Cu and Cu_2O–Cu quickly became dark-colored with a fast decline in current, which may have resulted from severe Cu oxidation and organic deposition on their surfaces, as evidenced by XPS and Raman analyses (Fig. 3c and S9). The surface hydroxyl groups (Cu–OH, 531.4 eV) of both $Cu(OH)_2$–Cu and Cu_2O–Cu also increased dramatically after 10 hours, while the peak for Cu_2O (530.4 eV) decreased, indicating there were changes in the

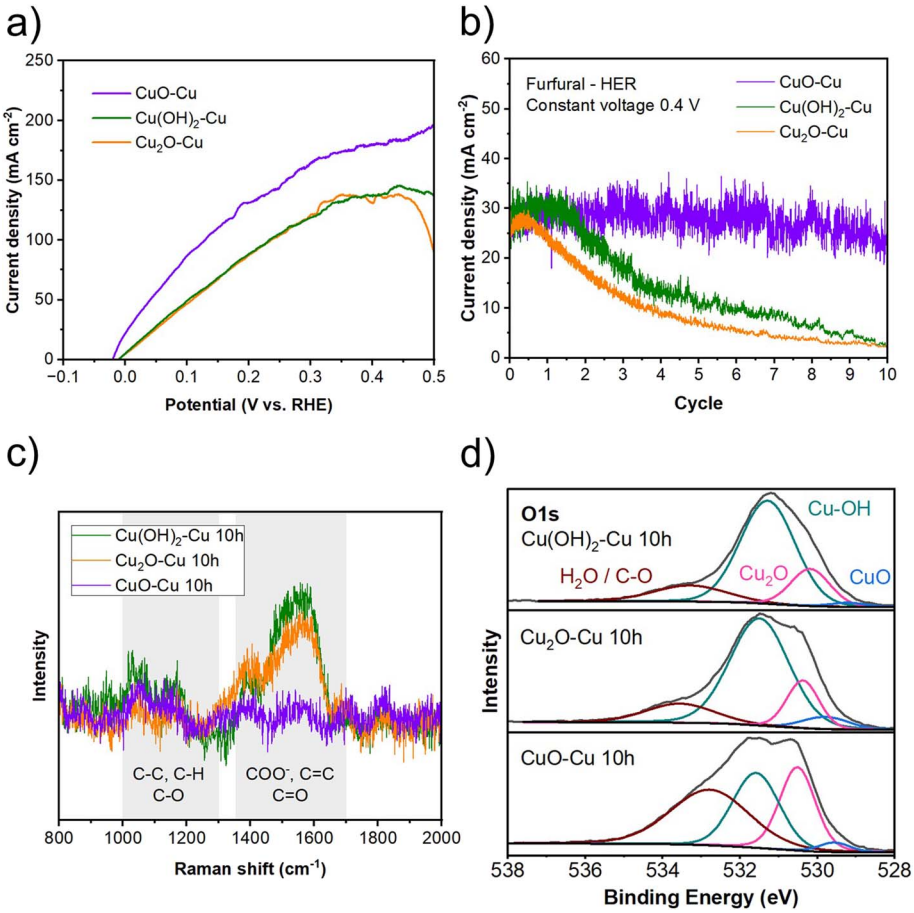

Fig. 3 Performance of the Cu electrocatalysts. (a) LSV curves of the three electrocatalysts in 0.1 M furfural and 2 M KOH. (b) Stability of the three electrocatalysts during 10 h single-pass flow electrolysis (furfural-HER, constant voltage of 0.4 V). Current densities using CuO–Cu decreased from 27 mA cm^{-2} to around 23 mA cm^{-2} after 10 h, while using $Cu(OH)_2$–Cu and Cu_2O–Cu, the current density reached around 2 mA cm^{-2}. (c) Raman spectra of the three electrocatalysts. Fewer aromatic absorption peaks were observed at CuO–Cu, which may partially be explained by the improved stability. (d) XPS O 1s peak-fitting results of the three electrocatalysts after a 10 h electrolysis. The three major O 1s peaks of CuO–Cu were well maintained after the 10 h electrolysis.

surface oxygen composition and its catalytic performance (compare Fig. 3d with the previous Fig. 2e). In contrast, CuO–Cu maintained a relatively constant current with much less darkening than the other two substrates. The ratio of the three O 1s peaks (lattice oxygen of Cu_2O and CuO, surface hydroxyl groups, and adsorbed oxygen) remained almost the same after 10 hours, showing the robustness of the catalyst. These results also evidence the importance of surface defects in mitigating organic deposition, consistent with similar cases in carbon dioxide reduction on Cu.[20,21] During catalyst preparation, CuO took much longer to be electrochemically reduced than Cu_2O, indicating the formation of much more defects to improve the furfural adsorption. Therefore, the CuO–Cu electrocatalyst was selected for further experiments. After 10 cycles, the actual hydrogen volume collected from the HER chamber reached 88% of the theoretical hydrogen volume calculated from the charge capacity (Fig. S10). This efficiency loss could be attributed to the overpotentials in the cell components, the HER catalytic activity, and the technical limitations of collecting small-sized hydrogen bubbles from the HER chamber. However, considering the simultaneously produced hydrogen at both the furfural and HER chambers, the average furfural-hydrogen conversion efficiency could reach 167% (Fig. S10). The furfural-hydrogen conversion efficiency was calculated based on the sum of hydrogen collected from both cell 1 and cell 2, divided by the theoretical volume of hydrogen calculated from the charged capacity of cell 1, as shown by the equation below:

$$\eta_{\text{total}} = (V_{\text{cell1}} + V_{\text{cell2}})/V_{\text{theo, cell1}} \times 100$$

where V_{cell1} and V_{cell2} are the actual hydrogen volumes collected from cell 1 and cell 2 and $V_{\text{theo, cell1}}$ is the theoretical volume of hydrogen calculated from the charged capacity of cell 1.

Furfural electrooxidation coupled with the HER using zinc mediation

In the three-chamber cell (Fig. 1), 0.1 M furfural in 2 M KOH was added at a flow rate of 50 mL min^{-1} using recirculation, and cell 1 was fixed at a constant voltage of 0.8 V during electrolysis (work model 1 in Fig. S11a). The maximum current density reached over 100 mA cm^{-2} but quickly decreased due to rapid

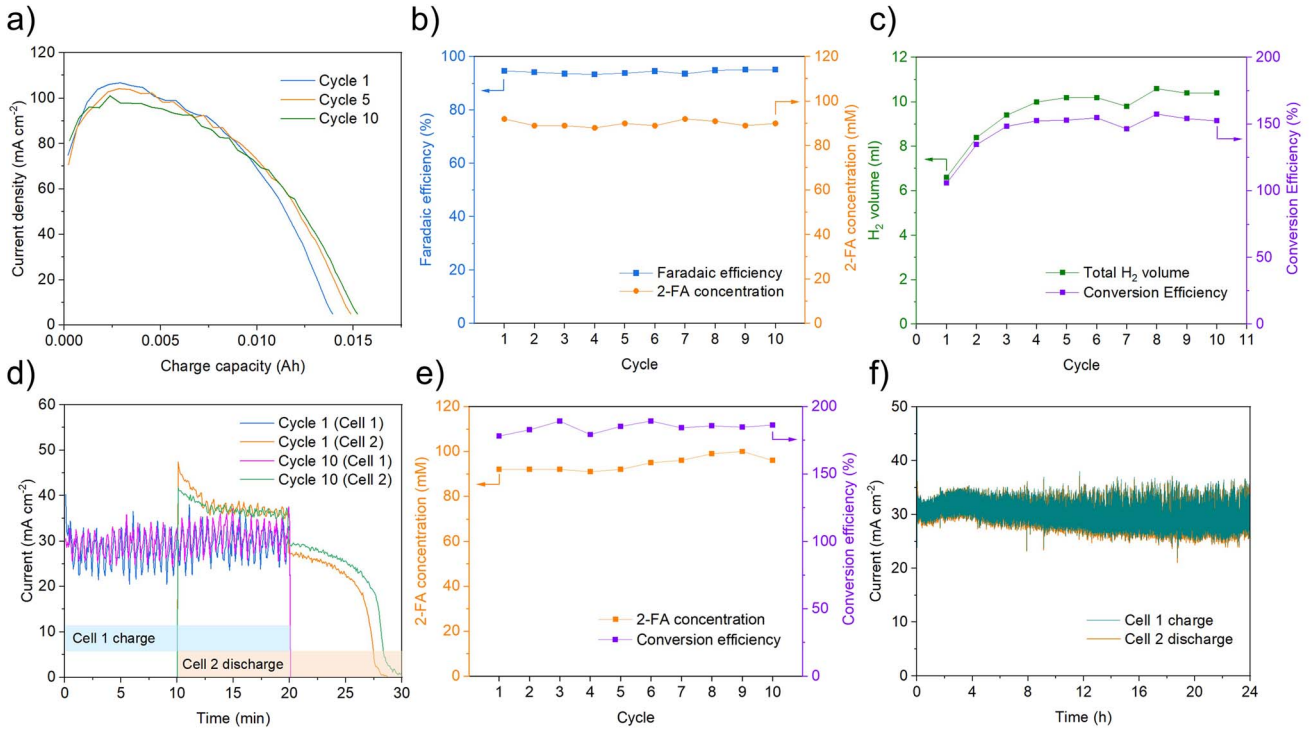

Fig. 4 Furfural-Zn-HER coupled electrolysis. (a) Current profiles of cell 1 during furfural-Zn coupling using CuO–Cu as a furfural catalyst. Cell 1 was given a constant cell voltage of 0.8 V immediately after 10 mL of furfural electrolyte was added as a batch. (b) Cell performance during 10 cycles: faradaic efficiencies between cell 1's charge capacity and cell 2's discharge capacity (blue) and 2-FA product concentrations sampled from cell 1 (orange). (c) Total hydrogen volume, assuming cell 1 produced the same amount of hydrogen as cell 2 (green) and furfural-hydrogen conversion efficiencies (purple). (d) Current of cells 1 and 2 during the first and 10th cycle (cell 2's discharge current is depicted as positive for comparison). Cell 2 started HER-discharge during the cell 1 charge step. Cell 1's current was not interrupted when starting cell 2. Furfural electrolyte was supplied in a single-pass flow. (e) 2-FA product concentrations sampled from cell 1 (orange) and furfural-hydrogen conversion efficiency (purple) over 10 cycles. (f) Current during cell 1–cell 2 simultaneous 24 h cycling of furfural-Zn-HER coupled electrolysis (cell 2 discharge current was depicted as positive for comparison).

furfural oxidation at a high flow rate (Fig. 4a). After cell 1 reached the cut-off current, cell 2 was discharged at a constant load of 1 ohm until reaching the cut-off of 0 V for complete zinc oxidation. The current of cell 2 was below 50 mA cm^{-2} and it maintained a relatively flat curve like that of a zinc-air battery (Fig. S12). Ten batches of 10 mL furfural were oxidized in series. The average faradaic efficiency between cell 1 and cell 2 was 94%, and the 2-FA yield was maintained at an average of 90% (Fig. 4b). The average current was slightly reduced after 10 cycles, which could be attributed to the morphological degradation of the catalysts.[11a] Assuming cell 1 produced the same amount of hydrogen as cell 2, the total hydrogen production from chamber 1 and chamber 3 increased after every cycle until reaching a limit of 10.4 mL (Fig. 4c), which was equivalent to around 152% of the theoretical H_2 volume calculated from the capacity charged at cell 1.

Cell 1 and cell 2 could also work independently to enhance the time efficiency by releasing hydrogen (cell 2) without stopping furfural oxidation (cell 1) (work model 2 in Fig. S11b). As shown in Fig. 4d, the HER-discharge was started 'during' the charge step in cell 1, making the two cell operations partially overlapped. Furfural electrolyte was supplied in a single-pass flow for continuous operation. For ten consecutive cycles, the charge step in cell 1 maintained a constant current of around 30 mA cm^{-2}, with current fluctuations due to hydrogen production on the CuO–Cu electrode at a low flow rate. The current in cell 1 was not disturbed by the current in cell 2 (see the current curves in Fig. 4d), showing the possibility of their independent operation. The 2-FA yield was maintained at above 95%, and the average furfural-hydrogen conversion efficiency was 184% (Fig. 4e). The average faradaic efficiency and furfural-hydrogen conversion efficiency were maintained similar to the previous batch experiments. To further evaluate the stability of the cells, a continuous simultaneous operation of cell 1 and cell 2 was also demonstrated for 24 hours (work model 3 in Fig. S11c). The two cells maintained almost identical currents since the zinc reduced in cell 1 was simultaneously oxidized in cell 2 (Fig. 4f). The 2-FA yield was maintained above 88% for 24 hours. Overall, the independence of the two cells in our three-chamber cell was verified, enabling time-efficient furfural and hydrogen production.

Furfural electrooxidation coupled with HER using soluble redox-active molecule mediation

Although zinc is advantageous in delivering a high discharge voltage due to its sufficiently low redox potential, it is always stored in a solid state, which limits its storage capacity. Zinc can

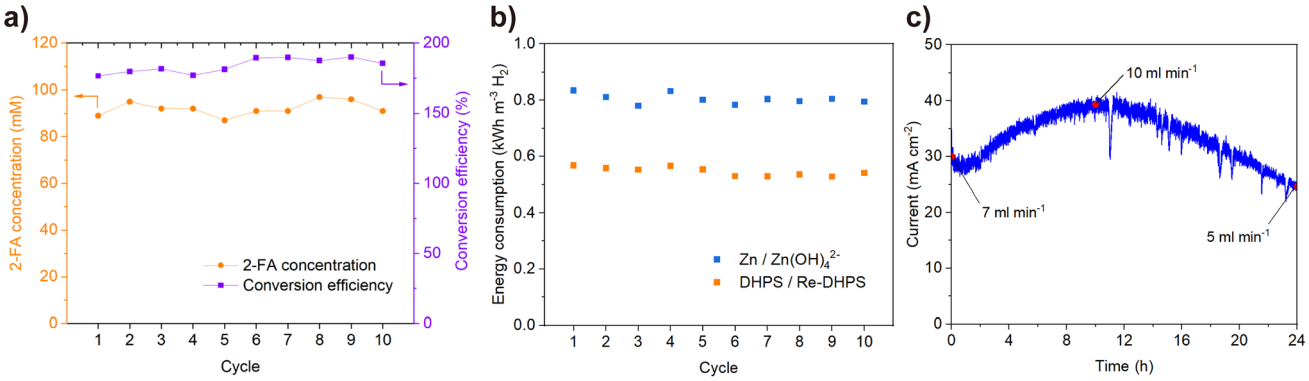

Fig. 5 Furfural-DHPS-HER coupled electrolysis. (a) 2-FA yield and furfural-hydrogen conversion efficiency for 10 cycles. DHPS was reduced to Re-DHPS at cell 1 at a constant cell voltage of 0.45 V (furfural-DHPS) and then re-oxidized in cell 2 (Pt/C-felt), chemically producing hydrogen. (b) Energy consumption per m^{-3} of H_2 compared with the previous Zn experiment results shown in Fig. 4b. (c) Cell 1 current and cell 2 hydrogen production rate during the 24 h electrolysis at a higher storage capacity (DHPS 0.5 M, 1 L). Test conditions were scaled accordingly (cell active area 4 → 36 cm^{-2}, flow rate 1 → 9 mL min^{-1}) to maintain the same current density and 2-FA yield.

also be replaced by soluble organic redox-active molecules to achieve higher energy-density hydrogen storage. As already shown in Fig. 1, the redox couples were reduced in a single electrochemical cell to oxidize furfural (cell 1), which was then sent to an external single-compartment cell assembled with Pt-coated felt (cell 2), where water was chemically oxidized to produce hydrogen and the molecules were re-oxidized to their original states. Various organic redox-active molecules have been reported recently for energy-storage applications.[22] Among them, DHPS and BHPC are considered water-soluble redox couples (Fig. S1), where much higher energy densities can be expected from them than zinc by reaching maximum solubilities of up to 1.8 M (DHPC) and 1.55 M (BHPC) in KOH solutions.[23] Both DHPS and BHPC have been reported to exhibit excellent capacity retention.[23b,c] Also, a stable, long cycle life is expected when using DHPS in an inert, light-proof environment.[24] During electrolysis, the electrolyte half-cell potential (the potential measured against a reference electrode) of Re-DHPS quickly reached below the HER potential around −0.83 V, causing the spontaneous chemical HER when in contact with the Pt catalyst (Fig. S13). The Re-BHPC (reduced state of BHPC) could also react with water when the half-cell potential of the electrolyte was below the HER potential. Both couplings indicated that spontaneous HER can be realized by utilizing electrolytes whose half-cell potential is below the HER potential. After the HER, the potential could turn back, enabling continuous circulation.

Furfural-DHPS cycling was performed by coupling a 0.1 M furfural single-pass flow with 0.1 M DHPS circulation. A constant voltage of 0.45 V was maintained for 20 minutes for each cycle, wherein the reduced state of DHPS (Re-DHPS) was pumped to an external Pt/C-cell for the chemical HER discharge. Ten consecutive cycles yielded 92% of 2-FA while maintaining the current at almost the same level (Fig. 5a and S14). The average furfural-hydrogen conversion efficiency reached around 184%, which was comparable to that from the furfural-HER two-electrode coupling (Fig. S15). Thanks to its lower reduction potential, DHPS-mediated cycling consumed 0.55 kWh m^{-3} H_2, representing a 32% lesser energy consumption per m^3 of hydrogen than the previous Zn-mediated cycling (Fig. 5b). A zero-gap cell (furfural-HER) using a thinner 25 μm membrane (Alkymer, w-25) further reduced the energy consumption down to 0.37 kWh m^{-3} H_2, which was comparable to a previous report[13] (Fig. S16). A continuous 24-hour electrolysis was performed using a higher storage capacity (DHPS 0.5 M, 1 L) and a larger cell active area (36 cm^2), wherein an average 2-FA yield of above 90% was maintained (Fig. 5c, Video S1). The current reached its maximum after around 10 hours, implying continuous activation of the catalyst over the large surface area during the electrolysis. Some current decay was observed afterwards, which could be attributed to organic deposition from the furfural/furoic acid and morphological degradation. Cleaning with ethanol could help to partially remove the surface deposition and restore the current and hydrogen production (Fig. S17). Assuming an average hydrogen production of 7.5 mL min^{-1} from both chamber 1 and chamber 3 for 24 hours, a total of 20 L of hydrogen was achieved while synthesizing more than 1.3 L of 2-FA. Therefore, a higher storage capacity can be expected when coupling liquid-phase redox molecules. However, mitigating molecule crossover between the chambers while minimizing the cell resistance remains a challenge. The DHPS-flowing chamber in the middle also requires compensation between the cell resistance and structural complexity. Therefore, future research may focus on reducing the cell resistance and extending the reaction path to allow operation at faster flow rates, thereby maximizing both the current density and 2-FA yield.

Conclusion

We have presented the concept of coupling 2-FA electrosynthesis with hydrogen production using zinc and DHPS mediation. A three-chamber cell was introduced to demonstrate separate or simultaneous charge–discharge cycling. Benefiting from the hydrogen production at two different chambers and

a highly stable oxide-derived CuO–Cu electrocatalyst, around 184% of furfural-hydrogen conversion efficiency was achieved. Changing zinc to DHPS allowed the oxidation to occur at a lower energy consumption, with the possibility of a higher storage capacity. Our novel concept introduced a new possibility for time-efficient furfural-hydrogen co-production.

Conflicts of interest

The authors declare no conflict of interest.

Data availability

All the data supporting this article are available within the article and its SI file.

Supplementary information including: LSV/CV plots, SEM images, XPS analysis, and other related data. See DOI: **https://doi.org/10.1039/d5ta03829d**.

Acknowledgements

The authors acknowledge the financial support from the Natural Science Foundation of China (No. 22209178 and 22279133), Liaoning Binhai Laboratory (No. LBLF202305 and LBLB202301), Energy Revolution S&T Program of Yulin Branch, the Dalian National Laboratory for Clean Energy, CAS (E411120705), and the LiaoNing Revitalization Talents Program (XLYC2403105). Prof. Xianfeng Li acknowledges the financial support from XPLORER PRIZE.

References

1 (*a*) H. Jin, J. Xu, H. Liu, H. Shen, H. Yu, M. Jaroniec, Y. Zheng and S.-Z. Qiao, *Sci. Adv.*, 2023, **9**, eadi7755; (*b*) J. Guo, Y. Zhang, A. Zavabeti, K. Chen, Y. Guo, G. Hu, X. Fan and G. K. Li, *Nat. Commun.*, 2022, **13**, 5046; (*c*) R. R. Beswick, A. M. Oliveira and Y. Yan, *ACS Energy Lett.*, 2021, **6**, 3167.

2 (*a*) K. de Kleijne, M. A. J. Huijbregts, F. Knobloch, R. van Zelm, J. P. Hilbers, H. de Coninck and S. V. Hanssen, *Nat. Energy*, 2024, **9**, 1139; (*b*) T. Terlouw, C. Bauer, R. McKenna and M. Mazzotti, *Energy Environ. Sci.*, 2022, **15**, 3583; (*c*) D. Hauglustaine, F. Paulot, W. Collins, R. Derwent, M. Sand and O. Boucher, *Commun. Earth Environ.*, 2022, **3**, 295.

3 (*a*) J. Wei, Y. Shao, J. Xu, F. Yin, Z. Li, H. Qian, Y. Wei, L. Chang, Y. Han, J. Li and L. Gan, *Nat. Commun.*, 2024, **15**, 9012; (*b*) J. Corbin, M. Jones, C. Lyu, A. Loh, Z. Zhang, Y. Zhu and X. Li, *RSC Adv.*, 2024, **14**, 6416.

4 (*a*) A. Hodges, A. L. Hoang, G. Tsekouras, K. Wagner, C.-Y. Lee, G. F. Swiegers and G. G. Wallace, *Nat. Commun.*, 2022, **13**, 1304; (*b*) S. Pan, H. Li, D. Liu, R. Huang, X. Pan, D. Ren, J. Li, M. Shakouri, Q. Zhang, M. Wang, C. Wei, L. Mai, B. Zhang, Y. Zhao, Z. Wang, M. Graetzel and X. Zhang, *Nat. Commun.*, 2022, **13**, 2294; (*c*) B. Rausch, M. D. Symes and L. Cronin, *J. Am. Chem. Soc.*, 2013, **135**, 13656; (*d*) M. Chen, N. Kitiphatpiboon, C. Feng, A. Abudula, Y. Ma and G. Guan, *eScience*, 2023, **3**, 100111.

5 J. Li and H. Duan, *Chem*, 2024, **10**, 3008.

6 (*a*) X. Lin, X. Xue and J. Du, *J. Mater. Chem. A*, 2024, **12**, 32095; (*b*) W.-J. Liu, Z. Xu, D. Zhao, X.-Q. Pan, H.-C. Li, X. Hu, Z.-Y. Fan, W.-K. Wang, G.-H. Zhao, S. Jin, G. W. Huber and H.-Q. Yu, *Nat. Commun.*, 2020, **11**, 265.

7 (*a*) X. Liu, M. Albloushi, M. Galvin, C. W. Schroeder, Y. Wu and W. Li, *Green Chem.*, 2024, **26**, 11351; (*b*) S. Kar, Q.-Q. Zhou, Y. Ben-David and D. Milstein, *J. Am. Chem. Soc.*, 2022, **144**, 1288.

8 (*a*) Z. Li, Y. Yan, S.-M. Xu, H. Zhou, M. Xu, L. Ma, M. Shao, X. Kong, B. Wang, L. Zheng and H. Duan, *Nat. Commun.*, 2022, **13**, 147; (*b*) D. Wang, P. Wang, S. Wang, Y.-H. Chen, H. Zhang and A. Lei, *Nat. Commun.*, 2019, **10**, 2796; (*c*) M. Huang, C. Cao, L. Liu, W. Wei, Q.-L. Zhu and Z. Huang, *eScience*, 2023, **3**, 100118.

9 (*a*) H. Ji, Z. Zhao, C. Zhang and X. Li, *Chem. Sci.*, 2024, **15**, 13185; (*b*) B. Garlyyev, S. Xue, J. Fichtner, A. S. Bandarenka and C. Andronescu, *ChemSusChem*, 2020, **13**, 2513; (*c*) H. Sun, X. Xu, L. Fei, W. Zhou and Z. Shao, *Adv. Energy Mater.*, 2024, **14**, 2401242.

10 G. Li, G. Han, L. Wang, X. Cui, N. K. Moehring, P. R. Kidambi, D. E. Jiang and Y. Sun, *Nat. Commun.*, 2023, **14**, 525.

11 (*a*) T. Wang, Z. Huang, T. Liu, L. Tao, J. Tian, K. Gu, X. Wei, P. Zhou, L. Gan, S. Du, Y. Zou, R. Chen, Y. Li, X. Z. Fu and S. Wang, *Angew Chem. Int. Ed. Engl.*, 2022, **61**, e202115636; (*b*) H. Liu, N. Agrawal, A. Ganguly, Y. Chen, J. Lee, J. Yu, W. Huang, M. Mba Wright, M. J. Janik and W. Li, *Energy Environ. Sci.*, 2022, **15**, 4175.

12 G. Fu, X. Kang, Y. Zhang, Y. Guo, Z. Li, J. Liu, L. Wang, J. Zhang, X.-Z. Fu and J.-L. Luo, *Nat. Commun.*, 2023, **14**, 8395.

13 T. Wang, L. Tao, X. Zhu, C. Chen, W. Chen, S. Du, Y. Zhou, B. Zhou, D. Wang, C. Xie, P. Long, W. Li, Y. Wang, R. Chen, Y. Zou, X.-Z. Fu, Y. Li, X. Duan and S. Wang, *Nat. Catal.*, 2021, **5**, 66.

14 C. Chen, Z. Fu, F. Qi, Y. Chen, G. Meng, Z. Chang, F. Kong, L. Zhu, H. Tian, H. Huang, X. Cui and J. Shi, *Angew Chem. Int. Ed. Engl.*, 2022, **61**, e202207226.

15 (*a*) Y. Feng, Q. Shi, J. Lin, E. Chai, X. Zhang, Z. Liu, L. Jiao and Y. Wang, *Adv. Mater.*, 2022, **34**, e2207747; (*b*) Y. Feng, L. Huang, Z. Xiao, X. Zhuang, T. S. Aslam, X. Zhang, Y.-X. Tan and Y. Wang, *J. Am. Chem. Soc.*, 2024, **146**, 7771.

16 J. Li, K. Ji, B. Li, M. Xu, Y. Wang, H. Zhou, Q. Shi and H. Duan, *Angew Chem. Int. Ed. Engl.*, 2023, **62**, e202304852.

17 M. Yang, Y. Li, C.-L. Dong, S. Li, L. Xu, W. Chen, J. Wu, Y. Lu, Y. Pan, Y. Wu, Y. Luo, Y.-C. Huang, S. Wang and Y. Zou, *Adv. Mater.*, 2023, **35**, 2304203.

18 E. Gioria, S. Li, A. Mazheika, R. Naumann d'Alnoncourt, A. Thomas and F. Rosowski, *Angew. Chem., Int. Ed.*, 2023, **62**, e202217888.

19 (*a*) C. Long, X. Liu, K. Wan, Y. Jiang, P. An, C. Yang, G. Wu, W. Wang, J. Guo, L. Li, K. Pang, Q. Li, C. Cui, S. Liu, T. Tan and Z. Tang, *Sci. Adv.*, 2023, **9**, eadi6119; (*b*) P. Hauke, T. Merzdorf, M. Klingenhof and P. Strasser, *Nat. Commun.*, 2023, **14**, 4708.

20 K. Xiang, F. Zhu, Y. Liu, Y. Pan, X. Wang, X. Yan and H. Liu, *Electrochem. Commun.*, 2019, **102**, 72.
21 J.-W. DuanMu, Z.-Z. Wu, F.-Y. Gao, P.-P. Yang, Z.-Z. Niu, Y.-C. Zhang, L.-P. Chi and M.-R. Gao, *Precis. Chem.*, 2024, **2**, 151.
22 (*a*) Z. Zhao, X. Liu, M. Zhang, L. Zhang, C. Zhang, X. Li and G. Yu, *Chem. Soc. Rev.*, 2023, **52**, 6031; (*b*) Z. Zhao, T. Li, C. Zhang, M. Zhang, S. Li and X. Li, *Nat Sustainability*, 2024, **7**, 1273; (*c*) M. Zhang, C. Mu, T. Li, C. Zhang and X. Li, *Adv. Energy Mater.n/a*, 2025, **15**, 2404813; (*d*) J. Zhang, Y. Zhang, J. Fu, X. Li and C. Zhang, *Electron*, 2024, **2**, e57.
23 (*a*) F. Zhang, H. Zhang, M. Salla, N. Qin, M. Gao, Y. Ji, S. Huang, S. Wu, R. Zhang, Z. Lu and Q. Wang, *J. Am. Chem. Soc.*, 2021, **143**, 223; (*b*) C. Wang, X. Li, B. Yu, Y. Wang, Z. Yang, H. Wang, H. Lin, J. Ma, G. Li and Z. Jin, *ACS Energy Lett.*, 2020, **5**, 411; (*c*) A. Hollas, X. Wei, V. Murugesan, Z. Nie, B. Li, D. Reed, J. Liu, V. Sprenkle and W. Wang, *Nat. Energy*, 2018, **3**, 508.
24 X. Xu, F. Sun, W. Tian, C. Zhang and X. Li, *Small Methods*, 2025, 2500477.

